Engineered Science
DOI: https://dx.doi.org/10.30919/es985

Improving the Corrosion Performance of LPBF- and EBM-Processed Ti-6Al-4V by Chemical Pickling

Alessandro Carrozza,[1, 2,*] Marina Cabrini,[1, 2] Sergio Lorenzi,[1, 2] Mariangela Lombardi[2, 3] and Tommaso Pastore[1, 2]

Abstract

Ti-6Al-4V is a popular material in the biomedical industry for orthopedic prosthetics production. Moreover, this alloy is well-processable via additive manufacturing (AM) technologies, allowing to tailor the design of the implant according to the specific needs of each individual patient. Nevertheless, AM technologies deploy metal powders, resulting in very rough topologies due to partially melted/adhered residual particles on the surfaces generated. Although this promotes osseointegration, corrosion-induced particle dropping can result in a severe inflammatory response in the patient. To overcome this, a pickling treatment was specifically developed and optimized to decrease the concentration of residual particles, without compromising surface roughness. Specimens produced via laser- and electron beam-powder bed fusion (PBF) were investigated. Three different surface finishing conditions (AM-generated, polished and pickled) were also compared via potentiostatic polarization tests. The specimens that underwent the pickling process proved to achieve lower current densities for long term exposures in simulated body fluid (SBF). Another critical phenomenon that occurs in prosthetics is the release of metal ions over time. To assess this issue, multiple electrochemical tests (potentiostatic polarization, electrochemical impedance spectroscopy) were deployed to assess the effect of the different PBF technologies and heat treatments on the ions release rate of Ti-6Al-4V in SBF.

Keywords: Additive manufacturing; LPBF; EBM; Ion release; Electrochemical characterization.
Received: 21 April 2023; Revised: 06 July 2023; Accepted: 08 July 2023.
Article type: Research article.

1. Introduction

Titanium alloys are materials characterized by high mechanical properties, low density and high corrosion resistance.[1] Among these alloys, Ti-6Al-4V is significantly more popular and represents the majority of the Ti market.[2] It is widely used in several industrial fields, such as aerospace,[3] automotive,[4] oil & gas,[5] and biomedical.[6] In this last sector the main applications are prosthetic implants (e.g., orthopedic, dental), for instance hip joints and knee replacements, and dental frameworks/bridges.[7] Here, the Ti-6Al-4V alloy is of particular interest due to its superior biocompatibility and biological/physiochemical properties. In fact, this alloy is particularly indicated when the colonization of the implant by natural human cells is required.[8]

Additive manufacturing (AM) processes are quickly gaining popularity in the biomedical sector for Ti-6Al-4V processing. These technologies allow the production of a component from a digital 3D design file via a layer by layer approach. Powder bed fusion (PBF) processes use a pre-alloyed powder as feedstock material. This is used to generate a powder bed and each layer is selectively melted according to the design desired. According to the heating source adopted to perform the melting operations, PBF technologies can be further categorized as laser powder bed fusion (LPBF) or electron beam melting (EBM), deploying a laser or electron beam, respectively.[9] The interest towards these techniques in the biomedical sector is related to multiple aspects. For instance, the possibility to customize the design in order to mimic the anatomy of the patient. This level of customization (complexity-for-free) is economically unfeasible with traditional manufacturing technologies.[10] Another advantage

[1] *Department of Engineering and Applied Sciences, University of Bergamo, Dalmine (BG) 24044, Italy.*
[2] *National Interuniversity Consortium of Materials Science and Technology (INSTM), Firenze 50121, Italy.*
[3] *Department of Applied Science and Technology, Politecnico di Torino, Torino 10129, Italy.*
**Email:* alessandro.carrozza@unibg.it (A. Carrozza)

of AM technologies lies in the possibility to create parts with a controlled porosity with the aim to match the elastic modulus of the human bones. By doing so, stress shielding phenomena can be avoided.[11] Additionally, PBF processes result in components characterized by a high surface roughness, due to the use of metal powders as feedstock material. This results in an increase of the specific area and improved osseointegration, thus a reduced recovery time needed for the patient after the surgical procedure. This aspect was investigated by Kayacan *et al.*[12] in a study where the osseointegration of AM-ed Ti-6Al-4V porous skull implants was investigated in sheep for 3 months. The authors demonstrated the formation of a good bond between the prosthetics and the surrounding tissues. Moreover, it is well-established in the literature that a rough material provides better adhesion performances with osseointegration-enhancing coatings, such as hydroxyapatite.[13]

Despite the high corrosion resistance of the Ti-6Al-4V alloy in biological environments due to its very stable electro-insulating passive layer, Ti and other alloying elements accumulation in the tissues around implants were reported by multiple studies. For instance, Schoon *et al.*[14] evaluated metals (Co, Cr and Ti) release from arthroplasty implants in the surrounding bone and bone marrow by deploying X-ray fluorescence and absorption techniques. Wu *et al.*[15] assessed the insurgence of localized corrosion phenomena of the Ti-6Al-4V alloy in a phosphate buffered saline solution with albumin, resulting in metal dissolution. Metal ions release events are also exacerbated by the adoption of PBF technologies, as these often results in implants with residual powder particles loosely attached to the surface. After implantation these particles are eventually released causing a significant and immediate increase in the amount of metals release in the body, possibly resulting in an inflammatory response. Despite the lack of proof of any titanium-induced adverse reaction in humans, the release of V and, most importantly, Al ions in the body is fundamental to assess due to its harmful effects.[16] In fact, the aluminum toxicity is well known, as its accumulation in the blood stream was correlated to Alzheimer's and Parkinson's diseases, as well as diabetic encephalopathy.[17] Some other adverse effect caused by Al ions accumulations are osteomalacia and pathological fractures.[18] Conversely, vanadium was linked to kidney damaging phenomena.[19] For these reasons, monitoring the ions release rate (irr) of Ti-6Al-4V implants in the human body is a necessary process to provide a long term benefit to the life of the patients. This parameter can be calculated using different experimental approaches. For instance, immersion tests, followed by a quantification of the ions released in the solution are possible. However, the quantities involved are usually so small that their measurement might be complicated. Another possible path is the use of electrochemical techniques, generally aimed at determining the corrosion resistance in a specific environment, in this case solutions that mimic the human body. For instance, Lee[20] investigated Ti-6Al-4V specimens in a Hank's solution via soaking in the test environment, and subsequently measuring the irr via inductively coupled plasma-mass spectrometry (ICP-MS). Conversely, Starosvetsky *et al.*[21] used potentiodynamic and potentiostatic tests to study PIRAC-nitrided Ti-6Al-4V samples. The authors evidenced that the samples that provided a lower anodic current were also characterized by a lower irr. Several works dealing with the electrochemical characterization of the AM-processed Ti-6Al-4V alloy can be found in the literature. For instance, Cabrini *et al.*[22] performed long term potentiostatic polarization tests to assess the behavior of different post-LPBF processing strategies on the corrosion performance of Ti-6Al-4V specimens. Chiu *et al.*[23] studied the tribo-electrochemical behavior of LPBF-ed samples via potentiodynamic polarization and corrosive wear tests. Nevertheless, only a very limited number of recent works performs a comparative analysis of the corrosion behavior of Ti-6Al-4V specimens produced via different AM technologies. For example, Metalnikov *et al.*[24] comparatively evaluated the effect of the microstructure on the susceptibility to corrosion via potentiodynamic polarization tests in a 0.9 M NaCl aqueous solution. Instead, Zadeh *et al.*[25] conducted electrochemical studies in a Ringer's solution. Additionally, no record of irr evaluations on AM-produced Ti-6Al-4V specimens via electrochemical characterization techniques are available in the literature, at the best of the authors' knowledge. Given the current literature gaps and the primary importance of the subjects discusses, in this work, a comparative analysis between EBM- and LPBF-produced Ti-6Al-4V samples were conducted. These were investigated both in the as-built and heat-treated states. Initially, a pickling treatment was optimized to minimize the number of residual powder particles on the surface of the specimens. Then, different electrochemical techniques were deployed to investigate the evolution of the irr along time in an environment that simulated the human body.

2. Materials and Methods

2.1 Specimen fabrication

All the specimens in this work were manufactured using an LPBF or EBM system. LPBF-produced samples were produced using an EOS M270 Dual Mode apparatus, characterized by a Yb fiber laser (maximum power of 200 W)

Table 1. Chemical compositions of the powders used for AM fabrication and relative sizes.

AM	Element (wt.%)								Particle sizes (μm)		
technology	Al	V	O	N	H	Ti	Fe	C	D(10)	D(50)	D(90)
EBM	6.41	3.86	0.09	0.01	0.002	Bal.	0.19	0.02	45	62	84
LPBF	5.86	3.99	0.083	0.003	0.002	Bal.	0.183	0.01	22	33	47

and operating in an Ar chamber to prevent oxidation. EBM-produced samples were manufactured using an Arcam A2X machine, working in a vacuum environment at a chamber temperature of approximately 700 °C. The feedstock material was a Ti-6Al-4V extra low interstitials (ELI) spherical powder in both cases. The relative compositions, as provided by the supplier, and particle size descriptors are provided in Table 1. The process parameters adopted for both systems were optimized and given by the producer of the machines and cannot be disclosed.

Some specimens were heat treated (HT) at 680 °C for 4h in a Pro.Ba VF800/S high-vacuum furnace. At the end of this process, the samples were allowed to cool inside the furnace at a cooling rate of approximately 2 °C/min.

2.2 Specimen design

A first batch of cylindrical specimens (5 mm height, 15 mm diameter) were fabricated for preliminary studies on the pickling treatment and microstructural investigations. All these were built with the circular faces perpendicular with respect to the building direction (Z).

A second batch of specimens were specifically designed for electrochemical testing (Fig. 1a). These were characterized by a central cylinder, representing the portion of the specimen (exposed area) that will be electrochemically tested, equal to 9.43 cm^2. The other cylindrical surfaces were inserted inside two insulating PTFE shafts, as shown in Fig. 1b. The electrical continuity for corrosion testing was granted by the coupling of a mechanical threaded inset on top of the specimen (M4, as shown in Fig. 1a) and a screw.

2.3 Pickling treatment

A pickling treatment was developed in order to decrease the concentration of the partially melted/adhered particles on the surfaces of the specimens. A 25% HNO_3 + 2.5% HF aqueous solution was used at room temperature. No stirring operations were performed. Different soaking periods were considered during the optimization process and the monitoring of the process over time was conducted via roughness measurements on 3D reconstructions of the exposed areas, obtained using a Sensofar S Neox 3D optical confocal profilometer. Sa and Sz were selected as suitable parameters to compare the surface features of the different samples, in compliance with ISO 25178. A 15×10 mm^2 area per samples was investigated, using a 10x magnification lens. 3D reconstructions of the surfaces were elaborated using the Mountains Maps Premium 7.4 software. The outcome of these evaluations was also used to determine the actual exposed area value per each specimen, taking into account the surface roughness.

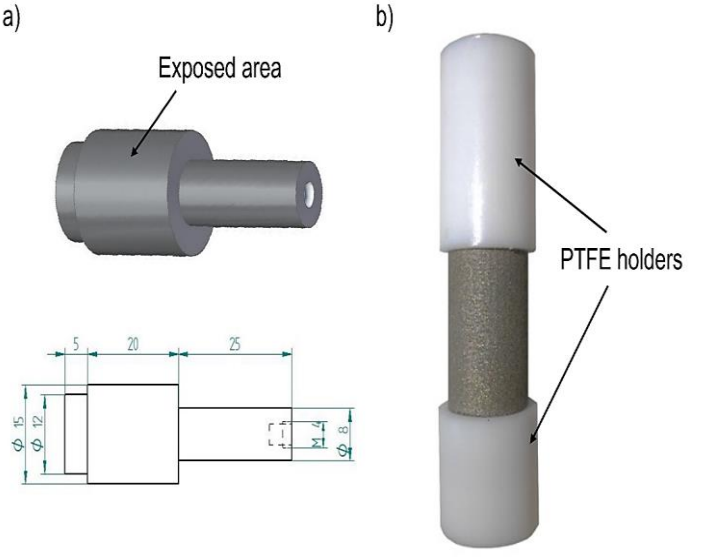

Fig. 1 Schematic representation of the specimens that underwent electrochemical tests (a) and relative slotting configuration of the PTFE holders.

2.4 Metallographic investigation

Some LPBF- and EBM-produced specimens in the as-built (AB) and HT states were mechanically cut along the Z direction for microstructural assessment. These samples were then mechanically ground with SiC papers up to a 2400 grit and then polished with a synthetic cloth paper and a colloidal silica solution. Chemical etching was performed to highlight the microstructures, using a Kroll solution (93% H_2O, 5% HNO_3 and 2% HF). The investigation of the microstructures was performed via optical imaging (OM) and scanning electron microscopy (SEM), using Leica 5000 M and Zeiss EVO 40 microscopes, respectively. Phase identification was conducted via X-ray diffraction (XRD). To do so, a PANalytical X-Pert Philips system was deployed. This apparatus was set to work in a Bragg Brentano configuration, operating at 40 kV and 40 mA. A Cu K_α radiation was used during the test.

2.5 Electrochemical tests

All the electrochemical tests were conducted in a simulated body fluid (SBF) solution (NaCl 8.74 g/L, NaHCO3 0.35 g/L, Na2HPO4·H2O 0.075 g/L, NaH2PO4·H2O 0.069 g/L), kept at 37°C. This environment was dearated via nitrogen bubbling for 1 h prior to the beginning of each experiment.

Potentiostatic tests were performed in 1L cell compliant with ASTM G5 standard, equipped with comprised two graphite counter electrodes and a saturated calomel electrode (SCE), as reference. A Luggin capillary was used in order to compensate the ohmic drop inside the testing apparatus. An Ivium CompactStat potentiostat was used to apply +500 mV vs SCE potential for the duration of the tests, whilst measuring the circulating current. This potential is slightly higher the value of titanium implants inside the human body.[26] At least two specimens per condition were tested for a duration of 150 – 200 h.

The electrochemical impedance spectroscopy (EIS) tests were performed in a 2.5 L cell, using a SCE as reference and a grid of mixed metal oxide titanium (MMO Ti) as a counter electrode. The open circuit potential (OCP) was monitored for 10 minutes before EIS test activation. After its stabilization, a sinusoidal polarization of 10 mV of amplitude in a frequency range of 0.0001÷40000 Hz was set, whilst collecting 10 frequency values each decade. These tests were performed using a Metrohm Autolab 302N potentiostat.

3. Results and Discussion

3.1 Optimization of the pickling treatment

The lateral surfaces of the EBM- and LPBF-processed samples were investigated using SEM imaging (Figs. 2a, d), revealing a highly irregular topology. This was mainly caused by the presence of quasi-spherical particles adhered to the surface of the specimens. The origin of this features lied in the manufacturing process. In fact, these surface irregularities were identified as partially adhered/melted powder particles. The surface finishing of the samples was measured via optical confocal imaging, as illustrated in Figs. 2b, e. This investigation clearly indicated that the EBM-produced samples were characterized by a rougher surface than the LPBF-processed ones. This outcome is consistent with the use of powder particles with a higher particle size distribution during the EBM process (see Table 1). This was further confirmed by the Abbott curves (Figs. 2c, f). In fact, the LPBF-manufactured specimens were characterized by a significantly narrower height distribution curve.

A pickling procedure was developed in order to decrease the amount or surface irregularities on the lateral surfaces of the samples. The optimization of the process was conducted via Sa measurements, performed after each minute soaking in the pickling solution until negligible variations were observed, as illustrated in Fig. 3.

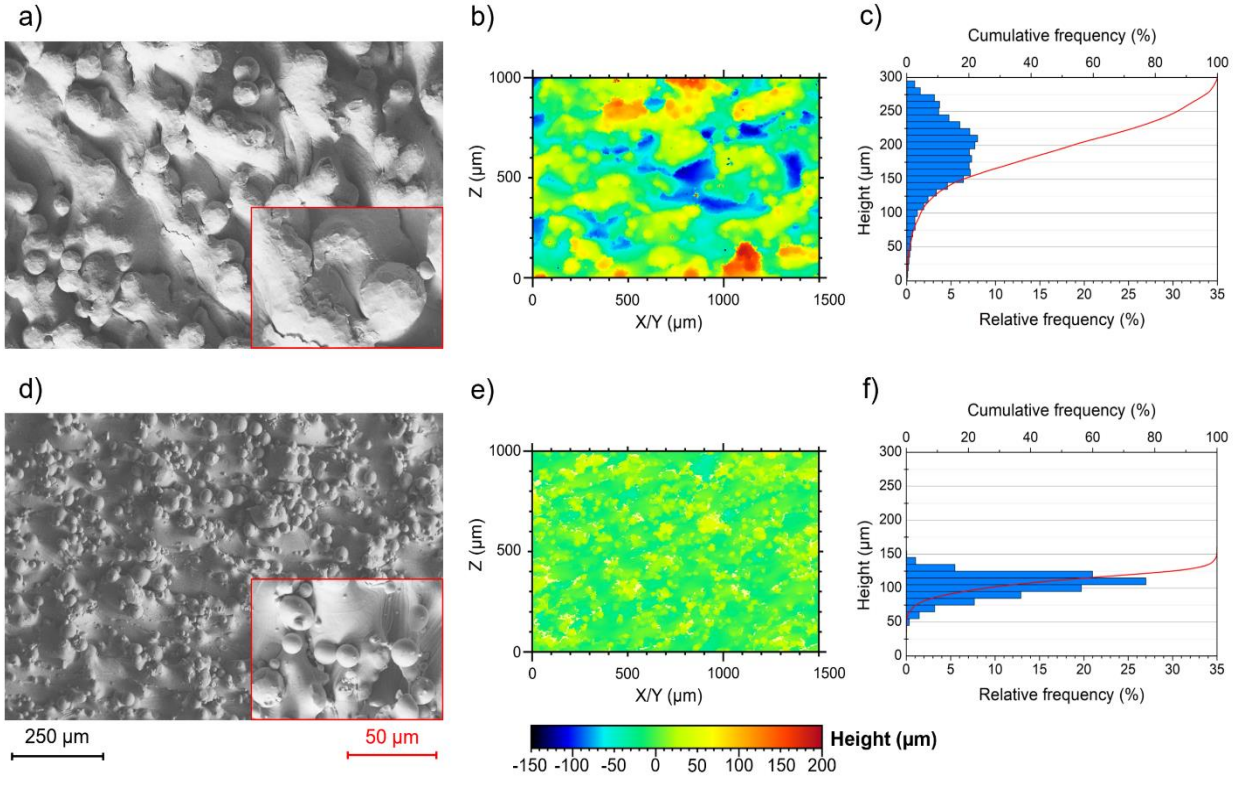

Fig. 2 SEM view of the lateral surfaces (a, d), confocal imaging reconstruction (b, e) and relative height distribution curve (c, f) of the EBM- and LPBF-processed specimens, respectively.

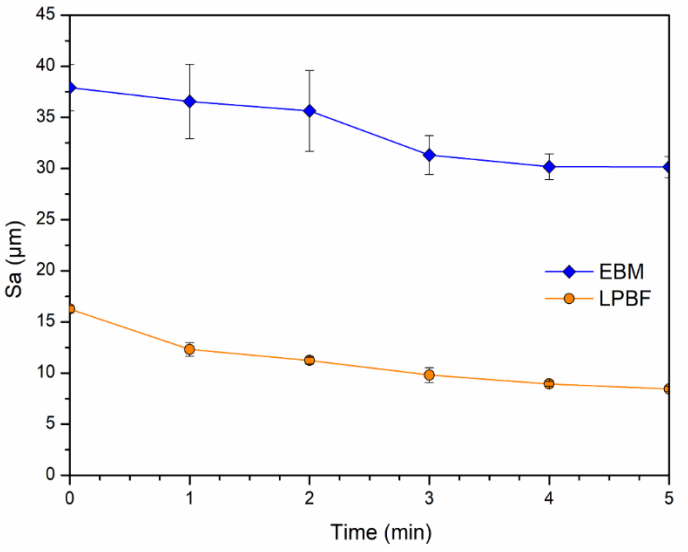

Fig. 3 Evolution of the Sa parameter at different immersion times in the pickling solution.

For both manufacturing processes the optimal pickling duration was found to be 5 cycles of 1 minute each, resulting in a total Sa decrease of 20.5% and 49.1% in the EBM- and LPBF-processed specimens, respectively (Table 2). It is also worth mentioning that the Sa standard deviation decreased for increasing cycle numbers. This is caused by the progressive removal of the larger particles from the surfaces, particularly evident in the EBM-processed specimens. The pickled samples (Figs. 4a, d) were characterized by surfaces still quite rough. Nevertheless, the number of residual particles was reduced, as testified by the confocal reconstruction maps and relative height distribution curves. Therefore, the detachment of the more loosely attached particles occurred. Conversely, the particles that were characterized by a stronger metallurgical bonding were able to sustain the pickling treatment. The overall decrease in the number of poorly adhered spheres was also confirmed by the confocal reconstruction of the lateral surfaces (Figs. 4b, e) and relative height distribution curves (Figs. 3c, f). The higher efficiency of the pickling treatment of the LPBF-manufactured samples

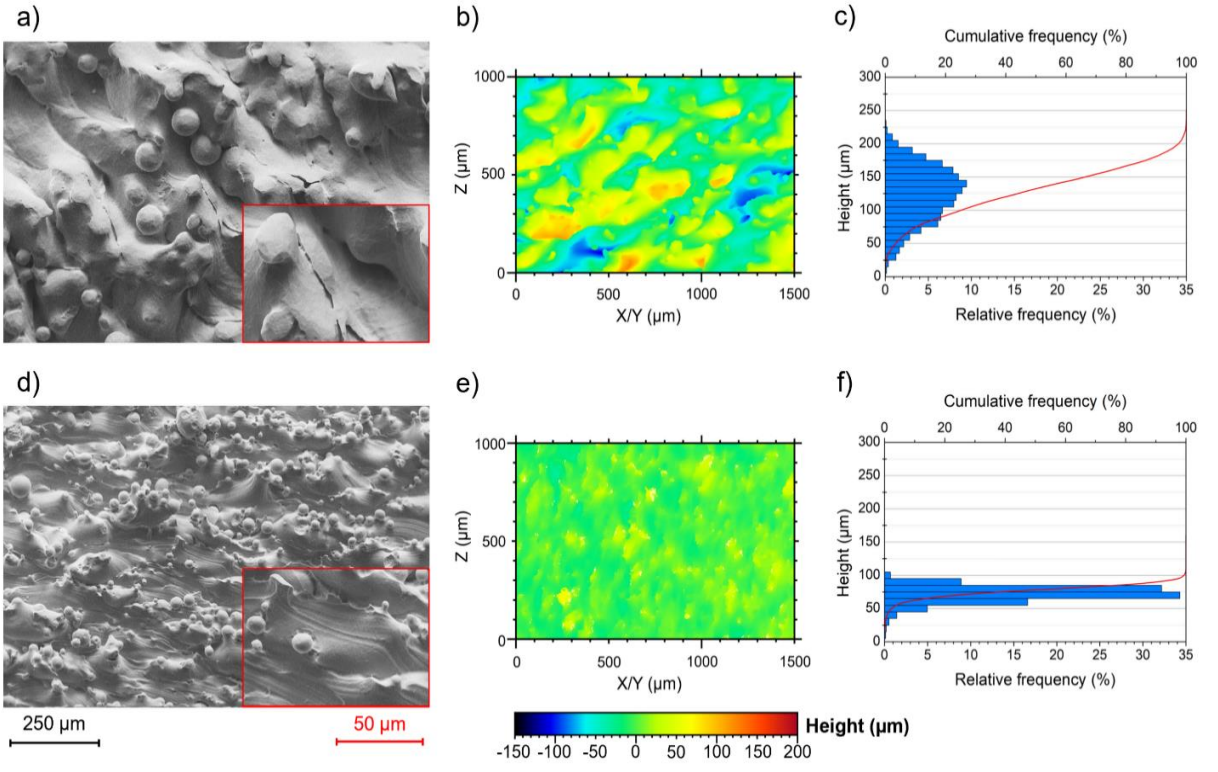

Fig. 4 SEM view of the lateral surfaces (a, d), confocal imaging reconstruction (b, e) and relative height distribution curve (c, f) of the pickled EBM- and LPBF-processed specimens, respectively.

can be related to the smaller particle size of the LPBF powders. In fact, the resulting particle/surface interaction area is minimized for small particles. Furthermore, the pre-sintering phase during EBM processing, occurring prior to the melting phase, and the high temperatures developed inside the chamber might contribute to the consolidation of the partially melted particles, increasing their adhesion with the surface of the specimens.[27]

Table 2. Effect of the pickling treatments on the surface parameters of the EBM- and LPBF-processed specimens.

Manufacturing technology	Surface finishing	Sz (μm)	Sa (μm)
EBM	AM-generated	340	40.7
	Pickled	251	33.7
LPBF	AM-generated	161	12.8
	Pickled	159	8.7

In general, the loss of the most loosely adhered powder particles is fundamental for biomedical implants due to their preferential detachment over long exposures. This phenomenon is fundamental to avoid, as it can cause a local inflammatory response.[28] Nevertheless, the persistence of a certain surface roughness is promising, the to the relative increase in terms of specific surface area, resulting in an increased activity with the surrounding area and osseointegration. Hence, the achievement of a surface finishing conditions that simultaneously promoted the interaction with the human body and prevents the detachment of hazardous metal particles appears optimal.

3.2 Influence of the surface condition on the corrosion behavior

Potentiostatic tests were conducted in order to investigate the influence of different surface finishing conditions on the AM-produced specimens, as illustrated in Fig. 5. The samples were characterized by an external surface in the AM-generated, polished and pickled states. Both AB and HT specimens were considered. All the combinations of conditions evidenced a decrease of the current density (i_c) over time. This behavior is associated with the growth of the electrically insulating oxide film on the surface of the Ti-6Al-4V alloy.[29] Moreover, this material shows a tendency to reach an asymptotic value of current density ($i_{c,\infty}$) over long immersion times, as demonstrated via long term potentiodynamic polarization tests by Cabrini *et al.*[22]. This value is significantly important due to its strict correlation with the irr.[30] Both the AB and HT specimens provided the following relationship:

$$i_{c,\infty}^{LPBF-generated} > i_{c,\infty}^{Polished} > i_{c,\infty}^{Pickled} \quad (1)$$

This phenomenon was associated with the quality of the protective oxide layer in the three different conditions. In fact, the lower protective quality of the high temperature-formed protective films is a well-known phenomenon, well documented in the literature. Hence, the worse behavior of the LPBF-generated condition is expected. During the pickling treatment, the complete dissolution of the hot-formed oxide occurs, causing the generation of a new, well-adherent and air-formed passive film, characterized by improved protective properties.[31] The comparatively higher $i_{c,\infty}$ of the polished specimens was correlated with the material removal occurring during the process. In fact, sub-superficial porosities, characterized by an internal hot-formed oxide layer, can become open porosities, due to the grinding of the material separating such defects from the outside. In this condition, the grinding process is expected to expose inner porosities of the AM-alloy and this effect cannot be avoided due to the very stochastic distribution of porosities in the material volume. The detrimental contribution of the emerging porosities on the corrosion resistance was already documented in a previous study by Sharma *et al.*[32] Therefore, the mechanical polishing process results in the formation of a new passive layer in most of the sample in addition to some spots where emerging porosities occur, thus providing an overall weaker oxide.

It is also worth noticing that the signal relative to the LPBF-generated specimens is characterized by a significant number of spikes with respect to the other conditions. In a previous work,[22] this effect was associated with the massive presence of unmelted particles, re-deposited on the specimen exposed surface. In fact, the particle/metal interface is a preferential corrosion path. As expected, spiking phenomena decreased after polishing and pickling treatments, due to the decrease in the amount of coarse unmelted particles.

The pickled samples provided the lower $i_{c,\infty}$ values, hence less critical irr, in this study. Moreover, as discussed before, the simultaneous high roughness, thus promoting osseointegration, and removal of the loosely adhered particles, thus preventing particle dropping, represent ideal combinations for biomedical implants applications. As a consequence of that, only the pickled specimens will be considered for further analyses in this work.

3.3 Materials characterization

A microstructure evaluation was performed on the AB and HT specimens in order to assess the influence of the AM technology and post-processing heat treatments on the materials investigated in this study, as illustrated in Fig. 6. Considering biomedical applications, a post-processing heat treatments appeared mandatory due to the mechanical

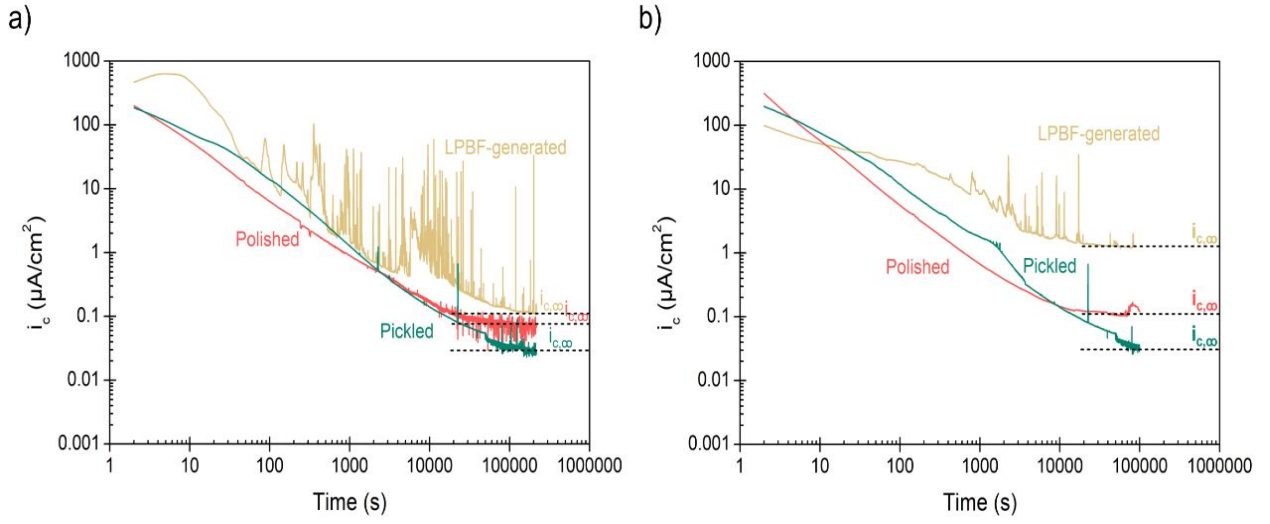

Fig. 5 Potentiostatic curves of the AB (a) and HT (b) LPBF-produced specimens.

performance required for the AM-produced Ti-6Al-4V alloy. In particular, a ductility ≥ 10% is needed per ASTM F2924. This value is usually not achieved in untreated LPBF-produced Ti-6Al-4V. For instance, Cao *et al.*[33] reported in a review that the vast majority of LPBF-processed specimens provided elongation values well below the threshold described in the standard. All the specimens in this work were characterized by columnar prior-β grains aligned parallel to the building direction (Z). This is a typical outcome in titanium alloys processed via PBF techniques, resulting from the epitaxial growth of the high temperature β grains. This phenomenon is mainly due to the conduction mode towards the building platform being the main heat dissipation mechanism during the process.[34] The EBM-processed specimens (Figs. 6a, b) provided a duplex α+β microstructure, with α lamellae mostly arranged in a Widmanstätten structure (±30/60°) and enveloped in a thin layer of β phase. These microstructural features are the results of the high chamber

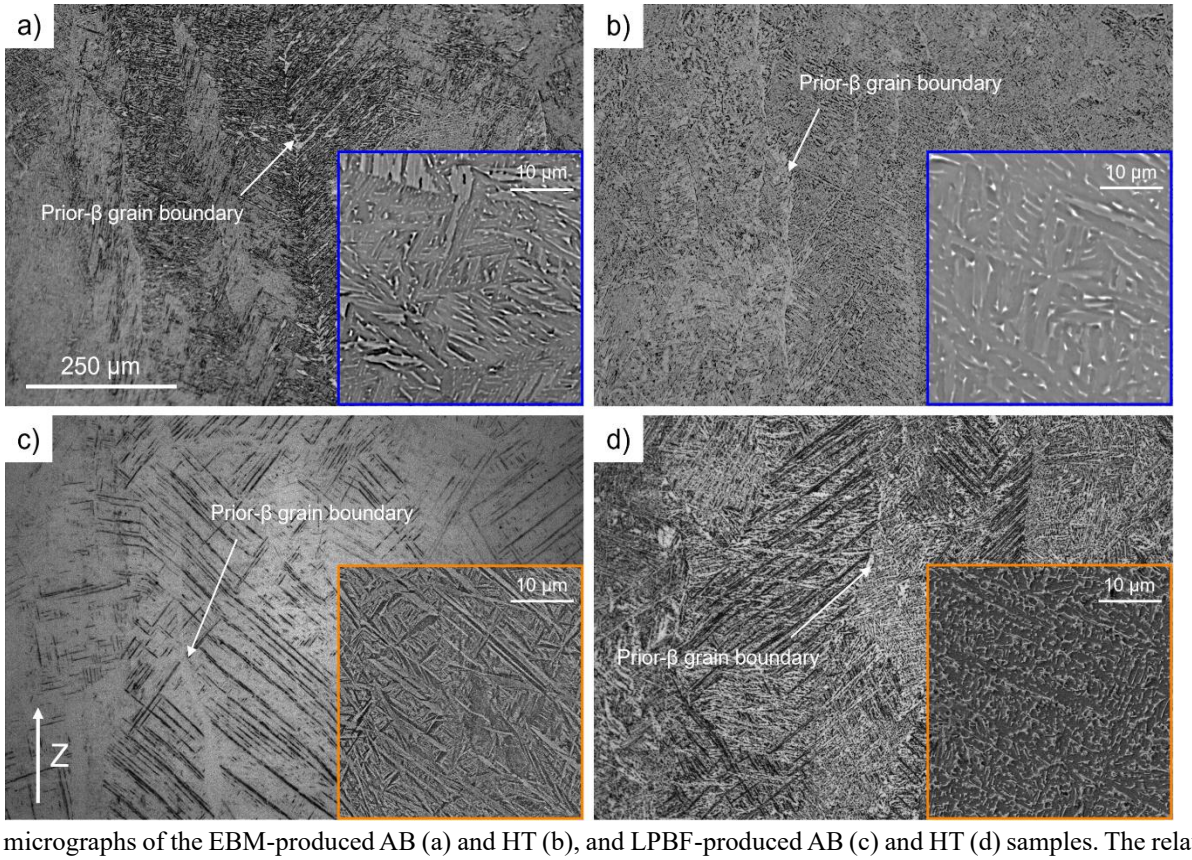

Fig. 6 OM micrographs of the EBM-produced AB (a) and HT (b), and LPBF-produced AB (c) and HT (d) samples. The relative SEM insets are also provided.

temperature (≃700°C), basically turning the whole process in a prolonged heat treatment. This phenomenon and the relative influence on the microstructural evolution of the alloy is further discussed in another publication.[27] General coarsening of the microstructure occurred after the heat treatment, but no other significant microstructure variations were highlighted. The AB LPBF-processed specimens (Fig. 6c) were characterized by a largely martensitic microstructure of α' needles. These laths were generated via the diffusionless β → α' transformation, given by the very high cooling rates achieved during the manufacturing process (≃ 10^5-10^7 °C/s). These values were obtained via computational modelling and successfully implemented in a microstructural evolution study by Pantawane *et al.*[35] Conversely, α' was completely decomposed in the HT LPBF-produced specimens (Fig. 6d), according to the diffusion-driven α' → α+β that leads to the release of the β-stabilizing elements (V) from the α cell.[36] However, in this case no basket-weave morphology was detected and the α lamellae were arranged in a fashion very similar to the pre-heat treatment α'.

Phase analyses were conducted via XRD to further corroborate the microstructural identifications, as illustrated in Fig. 7. Since the α and α' peaks are not distinguishable, the main β phase peak (2θ ≃ 40°) is commonly used to investigate whether the martensite decomposition occurred.[37] This peak lacked only in the AB LPBF-produced specimens, thus confirming that martensite decomposition occurred during the heat treatment.

3.4 Influence of PBF technology on the corrosion behavior

Representative potentiostatic curves of EBM- and LPBF-produced, AB and HT Ti-6Al-4V samples conducted in a SBF solution are reported in Fig. 8. All the conditions considered provided a decrease in terms of i_c over time. Roughly asymptotic values at $i_{c,\infty}$ = 0.01-0.07 μA/cm^2 were obtained after approximately 100 hours of immersion and polarization (Table 3). These numbers are in line with other data from the literature.[38] No significant differences related to the manufacturing process and/or heat treatment were appreciated. This outcome is in good agreement with a previous work,[22] where a homogenization of the film state, independently from the heat treatment, was stated over long exposure times in SBF. To further investigate the oxide growth dynamics and its evolution over time, EIS tests were conducted. Representative curves (1 day in SBF) are reported in Fig. 9. The phase curves are characterized by two well distinct peaks, in accordance with multiple works in the literature. The spectra can be fitted according to a well-established model of an equivalent circuit with two time-constants.[24] In this circu, the overall impedance of the passive film comprises different contribution that are related to the resistance and capacitance of the outer porous film, and the charge transfer resistance coupled with the double-layer capacitance, respectively. Constant phase elements are usually selected to better fit the inhomogeneity of the specimen's surface. In this specific model, the overall impedance describes the protection given by the passive film in response to the current applied to the system, that can be strictly linked to the amount of ions released in the environment. Under this consideration, the modulus values (|Z|) at low frequencies can be used as a mere indicator to estimate the resistance of the protective film to the current flow, giving rise to the release if metal ions. Only a slight effect can be noticed by comparing the different conditions considered, with LPBF-processed samples exhibiting the highest values of impedance modulus after early exposures.

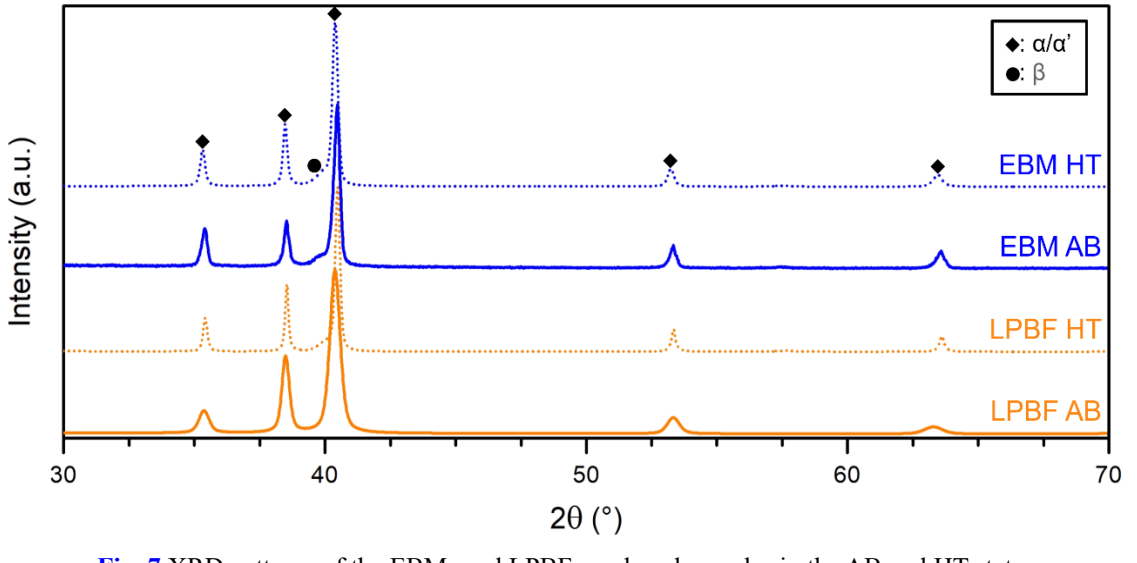

Fig. 7 XRD patterns of the EBM- and LPBF-produced samples in the AB and HT states.

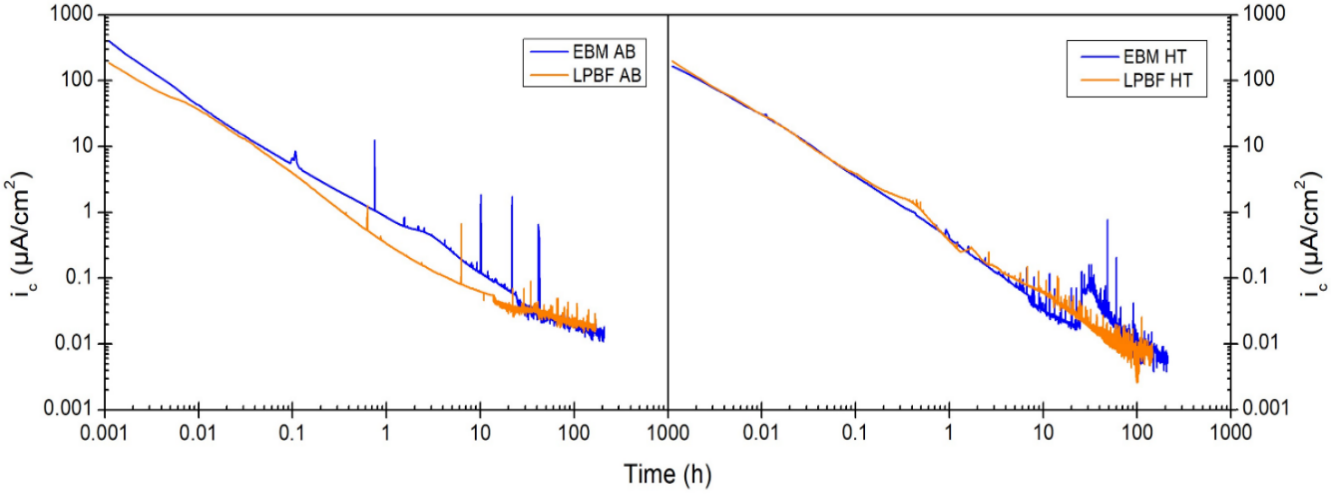

Fig. 8 Potentiostatic polarization curves (+ 500 mV vs SCE) of the EBM- and LPBF-produced Ti-6Al-4V samples in the AB and HT states.

Table 3. Average $i_{c,\infty}$ obtained via potentiostatic polarization tests.

Manufacturing technology	Heat treatment	$i_{c,\infty}$ (μA/cm²)*
EBM	AB	0.067 ± 0.004
	HT	0.020 ± 0.006
LPBF	AB	0.027 ± 0.007
	HT	0.123 ± 0.005

*Obtained by averaging the i_c values of the last 20 hours of test.

The evolution of the oxide layer was further assessed by performing the EIS tests after different immersion times (few hours, one day, one week, 5 months). A representative family of curves obtained (EBM-produced AB specimen) is provided in Fig. 10. An enlargement of the low-frequency phase peak (Fig. 10a) and an increase of the |Z| values at low frequencies are evident. Both these phenomena can be attributed to the modification of the passive film, as well as a significant increase in its overall protectiveness over the time. At very long exposures, the appearance of a third peak was also noticed. This behavior was associated to the sealing of the outer porous layer of the passive film and it is consistent with the increase in protectiveness over long exposure periods, as described by Pan *et al.*.[39] At longer exposures, the low frequency phase approaches values far from zero, meaning that the imaginary component of the impedance is high even at low frequencies. Under these circumstances, it is not possible to evaluate the effective value of the impedance modulus of the system as the mere resistance to current flow as the relaxation time of capacitors is very long, and the calculated impedance modulus is surely underestimated. Nevertheless, for the scope of this paper, this should be considered as a sufficiently accurate estimator of the amount of released ions and it is conservative as the underestimation

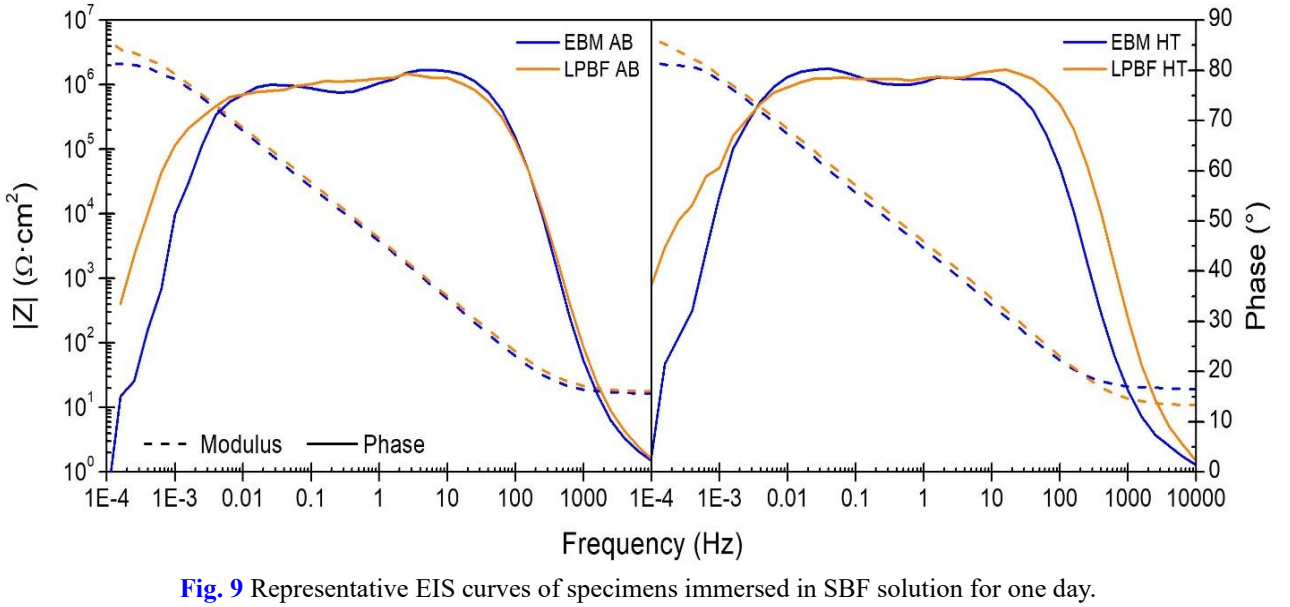

Fig. 9 Representative EIS curves of specimens immersed in SBF solution for one day.

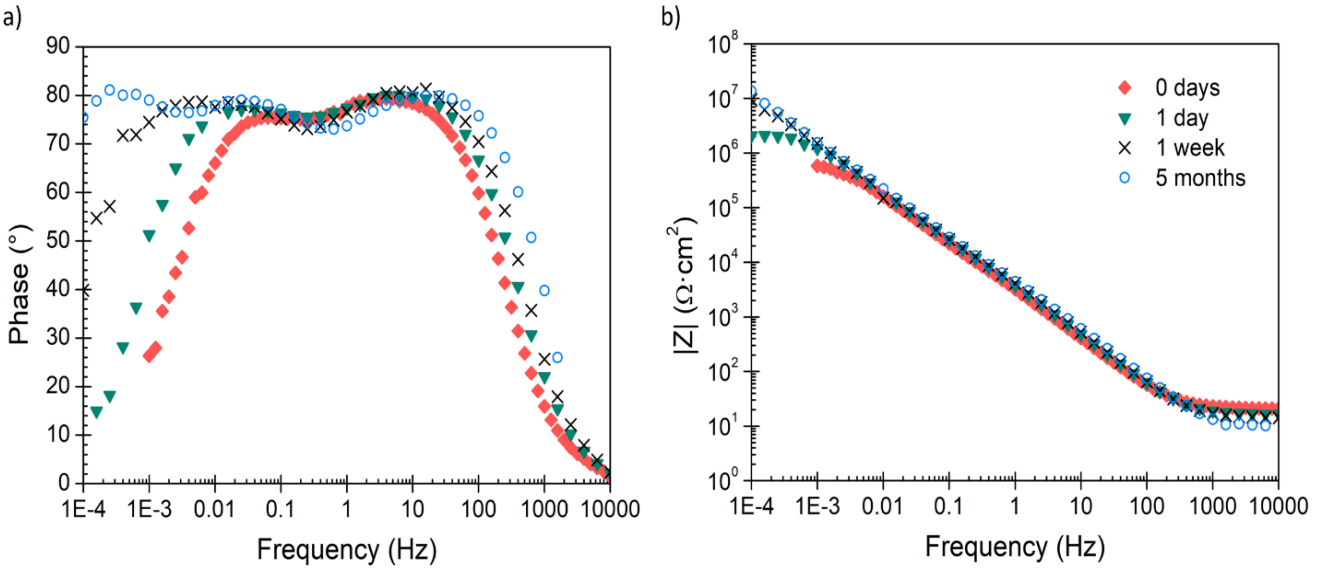

Fig. 10 Phase (a) and modulus (b) EIS curves, performed on EBM-produced specimens after different immersion times.

of the impedance modulus give rise to only a slight overestimation of the amount of released ions, especially at longer exposures.

Since both Potentiostatic polarization and EIS tests provide an outcome related to the passive film formation and growth kinetics, a correlation between these two techniques appears possible. In general, the former test can be considered to electrochemically estimate the irr. For instance, Buchanan *et al.*[40] deployed this technique to evaluate the wear-accelerated response of Ti-6Al-4V surgical implants, demonstrating that surface modification can substantially reduce the irr. Nevertheless, potentiostatic polarization is a destructive test, that also requires a current to circulate for a very prolonged time in the specimens. Conversely, EIS techniques are non-destructive and specimens can be kept in the solution for a long time without the necessity to constantly provide an input from an equipment. Therefore, the correlation of these aforementioned techniques can provide a more user-friendly way to determine the irr. To achieve that, the i_c values for a given immersion time, obtained via the potentiostatic polarization tests, were correlated to $|Z|^{-1}$ values at very low frequencies - approaching 10^{-4} Hz - from the EIS tests for the same immersion time. All the conditions (EBM-/LPBF-produced and AB/HT) were then considered altogether. This approach seemed to be appropriate, as no significant differences were evidenced by the EIS and potentiostatic tests, that can be related to the heat treatment and/or manufacturing technology. The outcome of this comparative evaluation is reported in Fig. 11. Since every point in this plot corresponds to a specific immersion time, the right part of the plot represents tests conducted on samples immersed in SBF for a shorter time. Overall, a good fit between the data was encountered. Therefore, EIS tests can be a valid and non-destructive alternative to potentiostatic polarization tests in order to evaluate the oxide growth of titanium specimens in SBF solution and the related irr.

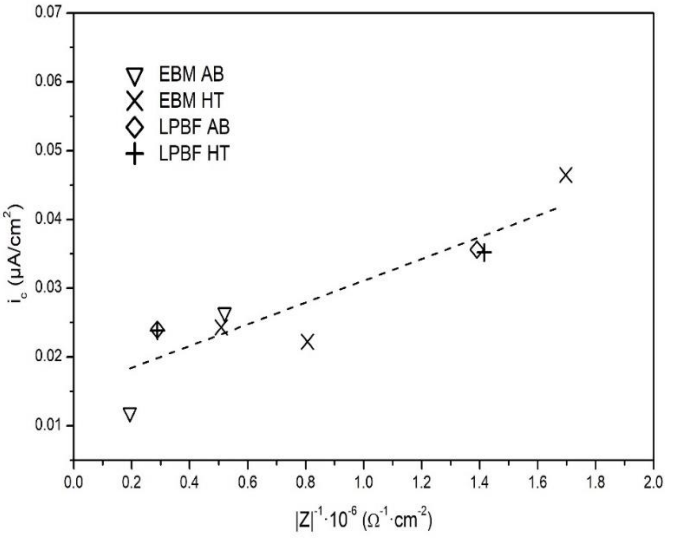

Fig. 11 i_c (potentiostatic test) vs $|Z|^{-1}$ (EIS test) relationship, relating data corresponding to the same immersion time.

3.5 Irr assessment

The estimation of the irr is possible via data gathered during the potentiostatic polarization investigation. In fact, the area under the i_c curve represent the total charge (Q) circulating for a given time (Fig. 12). This can be related to two separate effects: film formation and, most importantly, underlying metal dissolution.[41] Short term (ST) and long term (LT) exposure periods were considered. The threshold between these two conditions was 150 – 220 h (approximately 1 week), according to the potentiostatic test duration. This

categorization was made to distinguish the inflammatory response after the surgical procedure (1 week, ST) from the LT behavior.

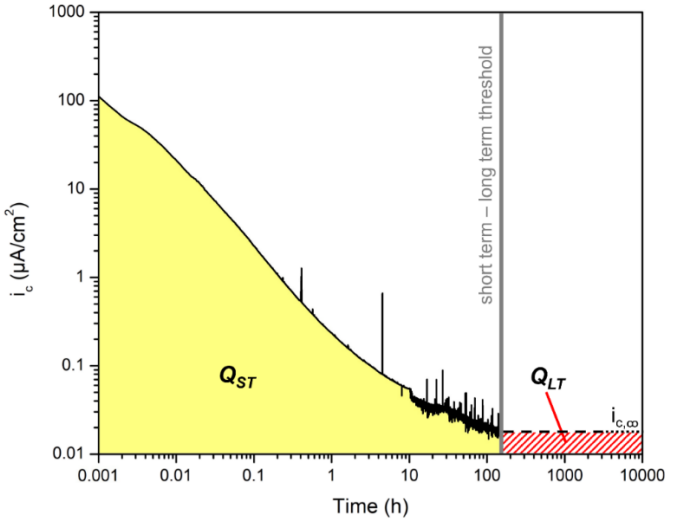

Fig. 12 Representative potentiostatic polarization curve with ST and LT areas highlighted.

Consequently, Q_{ST} and Q_{LT} were calculated using the following equations:

$$Q_{ST} = \int_0^{1\ week} i_c\, dt \quad (2)$$

$$Q_{LT} = i_{c,\infty} \cdot t \quad (3)$$

$$irr = \frac{m}{A} = \frac{M \cdot Q}{Z \cdot F} \quad (4)$$

The second Faraday law was then used to estimate the irr: Where A is the area of the specimen, M the equivalent atomic mass, Z the charge number and F is the Faraday constant (≃ $9.6 \cdot 10^4$ C/mol). Z values of 4, 3 and 5 for Ti, Al and V were used, respectively. The following ion distribution was considered: 70% Ti, 27% Al, 3% V (% at.). All these input data were gathered from a publication by Matykina *et al.*,[42] where the irr of Ti-6Al-4V specimens was measured via ICP-MS after 1, 4 and 8 weeks of immersion in a SBF solution.

The use of the Faraday law to estimate the irr was previously adopted by Díaz *et al.*[43] in commercially pure titanium (cp-Ti) samples. This technique is commonly adopted in the literature for coating thickness/removal determinations. For instance, Nordin *et al.*[44] adopted this approach to estimate the CrN coating dissolution after its electrochemically-induced corrosion. Instead, Zaidi *et al.*[45] used this method to evaluate the thickness of anodic alumina coatings on Al substrates, thus obtaining a good fit with the measurements performed via SEM imaging.

The outcome of the electrochemical evaluation of the irr is reported in Fig. 13 and Table 4. No significant difference in terms of irr_{ST} and irr_{LT} was evidenced between specimens characterized by different manufacturing technologies and/or heat treatments. A slightly lower irr during the first week from implantation was evaluated in the LPBF-built specimens, nonetheless further evaluation must be performed to confirm whether this is an actual phenomenon or a statistical effect. The irr_{ST} values found are coherent with other data from the literature, falling in a 16÷23 ng·cm^{-2}·day^{-1} range (Ti in SBF, 1 week immersion).[42,46,47] The immersion time required to for the irr_{LT} to match the irr_{ST} value was also estimated in the 11÷14 years range.

This electrochemical approach aimed at estimating the irr can prove to be a valid alternative to other conventional techniques, especially for estimating the effect of long time exposures without the necessity to test a material after years

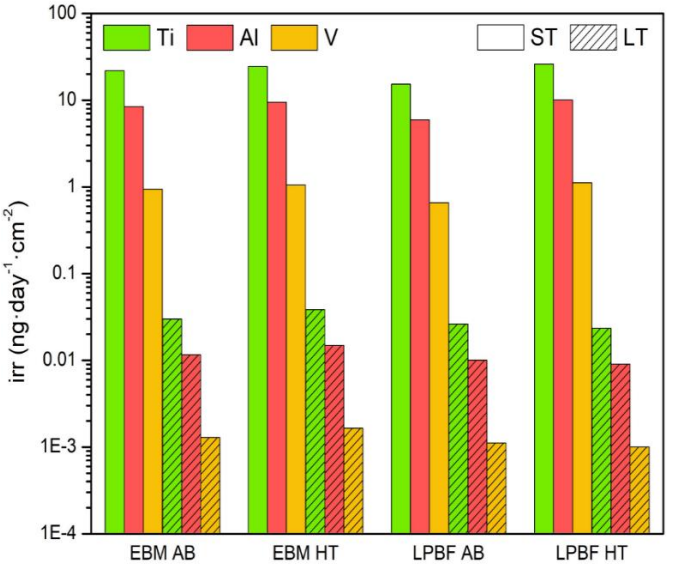

Fig. 13 Electrochemical investigation of the Ti, Al and V irr values for short (≃ 1 week) and long-term exposures in SBF solution.

Table 4. Daily ST and LT irr values and relative time required for the long-term exposure to achieve the first week values.

Manufacturing technology	Condition	$irr_{1\ week}$ (ng·cm^{-2}·day^{-1})			irr_{LT} (ng·cm^{-2}·day^{-1})			Time for irr_{ST} = irr_{LT} (years)
		Ti (Ti^{4+})	Al (Al^{3+})	V (V^{5+})	Ti (Ti^{4+})	Al (Al^{3+})	V (V^{5+})	
EBM	AB	21.99	8.48	0.94	0.0301	0.0116	0.0013	14
	HT	24.56	9.47	1.05	0.0386	0.0149	0.0016	12
LPBF	AB	15.40	5.94	0.66	0.0262	0.0101	0.0011	11
	HT	17.45	6.73	0.74	0.0235	0.0091	0.0010	14

of immersion. Nevertheless, further studies are required to increase the robustness of this work. In fact, comparisons with the literature are hardly conductible due to the great data scattering found, especially for longer immersion times.

4. Conclusions

In this work, Ti-6Al-4V ELI specimens were investigated via different electrochemical techniques, aimed at assessing their biomedical behavior, specifically for implants. LPBF and EBM were selected as suitable manufacturing technologies and comparatively analyzed. Moreover, the as-built and heat-treated states were also considered. A pickling treatment was specifically developed and optimized to remove a relevant number of partially melted/adhered metal particles from the surface of the samples after AM processing, without compromising the optima AM-generated surface morphology that promotes osseointegration. The pickling treatment is by itself necessary in order to prevent and/or mitigate the release of coarse particle during surgical intervention and after prothesis implantation. The main findings can be summarized as follows:

- The pickled samples demonstrated lower irrs over long periods compared to all other surface finishing conditions, as demonstrated by the lower current densities achieved for long period exposures.
- The growth of the passive layer in SBF solution was observed in both PS and EIS tests, confirming a reduction of irrs over long exposure periods
- A correlation was found between the outcome of the EIS and potentiostatic tests, indicating that EIS, a non-destructive assessment, can be a promising technique to study the long term corrosion behavior.
- Surface topology proved to be the most influencing parameter on the corrosion behavior and irr of the Ti-6Al-4V alloy in SBF solution. No significant effects related to the AM technology adopted of heat treatment were assessed. The estimated time required for the long period irr to match the inflammatory response (first week after implantation) was estimated between 11 and 14 years.

Acknowledgements

This research work has been funded by Regione Lombardia (Italy), regional law n° 9/2020, resolution n° 3776/2020.

Conflict of Interest

There is no conflict of interest.

Supporting Information

Not applicable.

References

[1] L. Casanova, M. Gruarin, M. Pedeferri, M. Ormellese, A comparison between corrosion performances of titanium grade 2 and 7 in strong reducing acids, *Materials and Corrosion*, 2021, **72**, 1506-1517, doi: 10.1002/maco.202112392.

[2] S. Liu, Y.C. Shin, Additive manufacturing of Ti6Al4V alloy: A review, *Materials & Design*, 2018, **164**, 8-12, doi: 10.1016/j.matdes.2018.107552.

[3] J. C. Williams, R. R. Boyer, Opportunities and issues in the application of titanium alloys for aerospace components, *Metals*, 2020, **10**, 705, doi: 10.3390/met10060705.

[4] A. K. Sachdev, K. Kulkarni, Z. Z. Fang, R. Yang, V. Girshov, Investigation of complex iron surface catalytic chemistry using the reaxff reactive force field method, *JoM*, 2012, **64**, 553-565, doi: 10.1007/s11837-012-.

[5] R. D. Kane, S. Craig, A. Venkatesh, Titanium alloys for oil and gas service: A review, NACE CORROSION 2009, NACE-09078.

[6] A. K. Sachdev, K. Kulkarni, Z. Z. Fang, R. Yang, V. Girshov, Titanium for automotive applications: challenges and opportunities in materials and processing, *JOM*, 2012, **64**, 553-565, doi: 10.1007/s11837-012-0310-8.

[7] E. Davoodi, H. Montazerian, R. Esmaeilizadeh, A. C. Darabi, A. Rashidi, J. Kadkhodapour, H. Jahed, M. Hoorfar, A. S. Milani, P. S. Weiss, A. Khademhosseini, E. Toyserkani, Additively manufactured gradient porous Ti-6Al-4V hip replacement implants embedded with cell-laden gelatin methacryloyl hydrogels, *ACS Applied Materials & Interfaces*, 2021, **13**, 22110-22123, doi: 10.1021/acsami.0c20751.

[8] L. A. Dobrzański, L. B. Dobrzański, A. Achtelik-Franczak, J. Dobrzańska, Application solid laser-sintered or machined Ti_6Al_4V alloy in manufacturing of dental implants and dental prosthetic restorations according to dentistry 4.0 concept, *Processes*, 2020, **8**, 664, doi: 10.3390/pr8060664.

[9] W. E. Frazier, Metal additive manufacturing: A review, *Journal of Materials Engineering and Performance*, 2014, **23**, 1917-1928, doi: 10.1007/s11665-014-0958-z.

[10] M. K. Niaki, S. Ali Torabi, F. Nonino, Why manufacturers adopt additive manufacturing technologies: the role of sustainability, *Journal of Cleaner Production*, 2019, **222**, 381-392, doi: 10.1016/j.jclepro.2019.03.019.

[11] Kaur, Ghadirinejad, Oskouei, An overview on the tribological performance of titanium alloys with surface modifications for biomedical applications, *Lubricants*, 2019, **7**, 65, doi: 10.3390/lubricants7080065.

[12] M.C. Kayacan, Y.B. Baykal, T. Karaaslan, K. Özsoy, İ. Alaca, B. Duman, Y.E. Delikanlı, Monitoring the osseointegration process in porous Ti6Al4V implants produced by additive manufacturing: an experimental study in sheep, *Journal of Applied Biomaterials & Functional Materials*, 2018, **16**, 68-75, doi: 10.5301/jabfm.5000385

[13] S. Arabnejad, R. B. Johnston, J. A. Pura, B. Singh, M. Tanzer, D. Pasini, High-strength porous biomaterials for bone replacement: A strategy to assess the interplay between cell morphology, mechanical properties, bone ingrowth and

manufacturing constraints, *Acta Biomaterialia*, 2016, **30**, 345-356, doi: 10.1016/j.actbio.2015.10.048.
[14] J. Schoon, B. Hesse, A. Rakow, M. J. Ort, A. Lagrange, D. Jacobi, A. Winter, K. Huesker, S. Reinke, M. Cotte, Metal-specific biomaterial accumulation in human peri-implant bone and bone marrow, *Advanced Science*, 2020, **7**, 2000412, doi: 10.1002/advs.202000412.
[15] J. Wu, M. Li, C. Lin, P. Gao, R. Zhang, X. Li, J. Zhang, K. Cai, Moderated crevice corrosion susceptibility of Ti_6Al_4V implant material due to albumin-corrosion interaction, *Journal of Materials Science & Technology*, 2022, **109**, 209-220, doi: 10.1016/j.jmst.2021.09.006.
[16] K. Afradh, G. Gopi, S. Shanmugasundaram, V. B. Krishnakumar Raja, Evaluation of serum metal ion levels in dental implant patients: a prospective study, *Annals of Maxillofacial Surgery*, 2021, **11**, 261, doi: 10.4103/ams.ams_70_21.
[17] J. Savory, O. Ghribi, Can studies of aluminum toxicity *in vivo* and *in vitro* provide relevant information on the pathogenesis and etiology of alzheimer's disease?, *Journal of Alzheimer's Disease*, 2007, **11**, 429-430, doi: 10.3233/jad-2007-11402.
[18] E. H. Jeffery, K. Abreo, E. Burgess, J. Cannata, J. L. Greger, Systemic aluminum toxicity: effects on bone, hematopoietic tissue, and kidney, *Journal of Toxicology and Environmental Health*, 1996, **48**, 649-666, doi: 10.1080/009841096161122.
[19] A. B. Goldfine, M.-E. Patti, L. Zuberi, B. J. Goldstein, R. LeBlanc, E. J. Landaker, Z. Y. Jiang, G. R. Willsky, C. R. Kahn, Metabolic effects of vanadyl sulfate in humans with non—insulin-dependent diabetes mellitus: *in vivo* and *in vitro* studies, *Metabolism*, 2000, **49**, 400-410, doi: 10.1016/s0026-0495(00)90418-9.
[20] T.-M. Lee, Effect of passivation and surface modification on the dissolution behavior and nano-surface characteristics of Ti-6Al-4V in Hank/EDTA solution, *Journal of Materials Science: Materials in Medicine*, 2006, **17**, 15-27, doi: 10.1007/s10856-006-6325-3.
[21] D. Starosvetsky, A. Shenhar, I. Gotman, Corrosion behavior of PIRAC nitrided Ti-6Al-4V surgical alloy, *Journal of Materials Science: Materials in Medicine*, 2001, **12**, 145-150, doi: 10.1023/a:1008922111376.
[22] M. Cabrini, A. Carrozza, S. Lorenzi, T. Pastore, C. Testa, D. Manfredi, P. Fino, F. Scenini, Influence of surface finishing and heat treatments on the corrosion resistance of LPBF-produced Ti-6Al-4V alloy for biomedical applications, *Journal of Materials Processing Technology*, 2022, **308**, 117730, doi: 10.1016/j.jmatprotec.2022.117730.
[23] T.-M. Chiu, M. Mahmoudi, W. Dai, A. Elwany, H. Liang, H. Castaneda, Corrosion assessment of Ti-6Al-4V fabricated using laser powder-bed fusion additive manufacturing, *Electrochimica Acta*, 2018, **279**, 143-151, doi: 10.1016/j.electacta.2018.04.189.
[24] P. Metalnikov, G. Ben-Hamu, D. Eliezer, Corrosion behavior of AM-Ti-6Al-4V: a comparison between EBM and SLM, *Progress in Additive Manufacturing*, 2022, **7**, 509-520, doi: 10.1007/s40964-022-00293-8.
[25] M. K. Zadeh, M. Yeganeh, M. T. Shoushtari, H. Ramezanalizadeh, F. Seidi, Microstructure, corrosion behavior, and biocompatibility of Ti-6Al-4 V alloy fabricated by LPBF and EBM techniques, *Materials Today Communications*, 2022, **31**, 103502, doi: 10.1016/j.mtcomm.2022.103502.
[26] J. B. Cotton, P. C. S. Hayfield, Decorative finishes on titanium, *Transactions of the IMF*, 1967, **45**, 48-52, doi: 10.1080/00202967.1967.11870018.
[27] A. Carrozza, G. Marchese, A. Saboori, E. Bassini, A. Aversa, F. Bondioli, D. Ugues, S. Biamino, P. Fino, Effect of aging and cooling path on the super β-transus heat-treated Ti-6Al-4V alloy produced via electron beam melting (EBM), *Materials*, 2022, **15**, 4067, doi: 10.3390/ma15124067.
[28] J. C. Tang, J. P. Luo, Y. J. Huang, J. F. Sun, Z. Y. Zhu, J. Y. Xu, M. S. Dargusch, M. Yan, Immunological response triggered by metallic 3D printing powders, *Additive Manufacturing*, 2020, **35**, 101392, doi: 10.1016/j.addma.2020.101392.
[29] J. Xing, Z. Xia, J. Hu, Y. Zhang, L. Zhong, Time dependence of growth and crystallization of anodic titanium oxide films in potentiostatic mode, *Corrosion Science*, 2013, **75**, 212-219, doi: 10.1016/j.corsci.2013.06.004.
[30] N. Cruz, J. Gil, M. Punset, J. M. Manero, J. P. Tondela, P. Verdeguer, C. Aparicio, E. Rúperez, Relevant aspects of piranha passivation in Ti_6Al_4V alloy dental meshes, *Coatings*, 2022, **12**, 154, doi: 10.3390/coatings12020154.
[31] T. Shibata, Y.-C. Zhu, The effect of film formation conditions on the structure and composition of anodic oxide films on titanium, *Corrosion Science*, 1995, **37**, 253-270, doi: 10.1016/0010-938x(94)00133-q.
[32] A. Sharma, M. C. Oh, J.-T. Kim, A. K. Srivastava, B. Ahn, Investigation of electrochemical corrosion behavior of additive manufactured Ti-6Al-4V alloy for medical implants in different electrolytes, *Journal of Alloys and Compounds*, 2020, **830**, 154620, doi: 10.1016/j.jallcom.2020.154620.
[33] S. Cao, Y. Zou, C. V. S. Lim, X. Wu, Review of laser powder bed fusion (LPBF) fabricated Ti-6Al-4V: process, post-process treatment, microstructure, and property, *Light: Advanced Manufacturing*, 2021, **2**, 2-20, doi: 10.37188/lam.2021.020.
[34] A. Carrozza, A. Aversa, P. Fino, M. Lombardi, Towards customized heat treatments and mechanical properties in the LPBF-processed Ti-6Al-2Sn-4Zr-6Mo alloy, *Materials & Design*, 2022, **215**, 110512, doi: 10.1016/j.matdes.2022.110512.
[35] M. V. Pantawane, S. Dasari, S. A. Mantri, R. Banerjee, N. B. Dahotre, Rapid thermokinetics driven nanoscale vanadium clustering within martensite laths in laser powder bed fused additively manufactured Ti_6Al_4V, *Materials Research Letters*, 2020, **8**, 383-389, doi: 10.1080/21663831.2020.1772396.
[36] E. Sallica-Leva, R. Caram, A. L. Jardini, J. B. Fogagnolo, Ductility improvement due to martensite α' decomposition in porous Ti-6Al-4V parts produced by selective laser melting for orthopedic implants, *Journal of the Mechanical Behavior of Biomedical Materials*, 2016, **54**, 149-158, doi: 10.1016/j.jmbbm.2015.09.020.
[37] A. Carrozza, A. Aversa, F. Mazzucato, M. Lombardi, S. Biamino, A. Valente, P. Fino, An innovative approach on directed energy deposition optimization: a study of the process

environment's influence on the quality of Ti-6Al-4V samples, *Applied Sciences*, 2020, **10**, 4212, doi: 10.3390/app10124212.
[38] R. Narayanan, S. K. Seshadri, Point defect model and corrosion of anodic oxide coatings on Ti-6Al-4V, *Corrosion Science*, 2008, **50**, 1521-1529, doi: 10.1016/j.corsci.2008.02.023.
[39] J. Pan, D. Thierry, C. Leygraf, Electrochemical impedance spectroscopy study of the passive oxide film on titanium for implant application, *Electrochimica Acta*, 1996, **41**, 1143-1153, doi: 10.1016/0013-4686(95)00465-3.
[40] R. A. Buchanan, E. D. Rigney Jr, J. M. Williams, Ion implantation of surgical Ti-6Al-4V for improved resistance to wear-accelerated corrosion, *Journal of Biomedical Materials Research*, 1987, **21**, 355-366, doi: 10.1002/jbm.820210308.
[41] S.R. Sousa, M.A. Barbosa, Effect of hydroxyapatite thickness on metal ion release from Ti6Al4V substrates, *Biomaterials*, 1996, **17**, 397-404, doi: 10.1016/0142-9612(96)89655-4.
[42] E. Matykina, R. Arrabal, B. Mingo, M. Mohedano, A. Pardo, M.C. Merino, In vitro corrosion performance of PEO coated Ti and Ti6Al4V used for dental and orthopaedic implants, *Surface and Coatings Technology*, 2016, **307**, 1255-1264, doi: 10.1016/j.surfcoat.2016.08.018.
[43] I. Díaz, M.Á. Pacha-Olivenza, R. Tejero, E. Anitua, M.L. González-Martín, M.L. Escudero, M.C. García-Alonso, Corrosion behavior of surface modifications on titanium dental implant. In situ bacteria monitoring by electrochemical techniques, *Journal of Biomedical Materials Research Part B: Applied Biomaterials*, 2018, **106**, 997-1009, doi: 10.1002/jbm.b.33906.
[44] M. Nordin, M. Herranen, S. Hogmark, Influence of lamellae thickness on the corrosion behaviour of multilayered PVD TiN/CrN coatings, *Thin Solid Films*, 1999, **348**, 202-209, doi: 10.1016/S0040-6090(99)00192-3.
[45] S. M. J. Zaidi, M. Z. Butt, F. Bashir, A comparative study of the anodic alumina film thickness measured via SEM and evaluated using Faraday's Law, *Materials Research Express*, 2019, **6**, 046404, doi: 10.1088/2053-1591/aafa08.
[46] M.C. Advincula, D. Petersen, F. Rahemtulla, R. Advincula, J.E. Lemons, Surface analysis and biocorrosion properties of nanostructured surface sol–gel coatings on Ti6Al4V titanium alloy implants, *Journal of Biomedical Materials Research Part B: Applied Biomaterials*, 2007, **80**, 107-120, doi: 0.1002/jbm.b.30575.
[47] M. Mohedano, E. Matykina, R. Arrabal, A. Pardo, M.C. Merino, Metal release from ceramic coatings for dental implants, *Dental Materials*, 2014, **30**, 28-40, doi: 10.1016/j.dental.2013.12.011

